Journal of Engineering Research and Reports

13(2): 1-10, 2020; Article no.JERR.57147
ISSN: 2582-2926

Simple Optical Measurements of Pre-treated Surface Roughness for Thermal Spray

Yukihiko Yamagata[1*], Ryo Iwasaka[1], Keita Shigyo[2], Juntaro Tanaka[2], Yasuyuki Kawaguchi[2] and Katsunori Muraoka[1,2]

[1]Interdisciplinary Graduate School of Engineering Sciences, Kyushu University, Kasuga-koen, Kasuga, Fukuoka 816-8580, Japan.
[2]Plazwire Co., LTD. 2-3-54 Higashi-naka, Hakata-ku, Fukuoka 812-0892, Japan.

Authors' contributions

This work was carried out in collaboration among all authors. Author YY designed the experimental equipment, performed the experiment, interpreted the obtained results, by which he made the major contribution of the whole work. Author RI carried out the experiment and contributed in interpreting the obtained results. Authors KS and JT measured surface roughness using a surface roughness tester and contributed in comparing the obtained results with those from the present experiment. Author YK managed the overall project and carried out literature searches. Author KM proposed the present research, contributed in interpreting the obtained result and wrote the draft of the article. All authors read and approved the final manuscript.

Article Information

DOI: 10.9734/JERR/2020/v13i217095
Editor(s):
(1) Dr. Guang Yih Sheu, Chang-Jung Christian University, Taiwan.
Reviewers:
(1) SaadAlbawi, University of Diyala, Iraq.
(2) Maria Lúcia Pereira da Silva, University of São Paulo, Brazil.
Complete Peer review History: http://www.sdiarticle4.com/review-history/57147

Original Research Article

Received 17 March 2020
Accepted 23 May 2020
Published 01 June 2020

ABSTRACT

For achieving satisfactory performance of coating layers obtained using the thermal spray technique, pre-treatments are carried out by roughening the smooth surfaces of metals to more than a few tens of μm. Although a surface roughness tester is reliable for quantitatively measuring the surface roughness, it requires expertise and a long measuring time. In the present article, a simple optical method is presented which the authors hope will replace the above surface roughness tester. The proposed method relies on first projecting a narrow beam of light from a light-emitting diode obliquely over the roughened surface, and then on measuring the distortion of the light as observed perpendicular to the surface. Proof-of-principle experiments were performed first against a surface roughness comparator, and then against actual blasted surfaces using both the optical method and the surface roughness tester, yielding the two methods to be in good agreement.

**Corresponding author: Email: yamagata@asem.kyushu-u.ac.jp;*

Keywords: Surface roughness; roughness parameter; optical measurement; LED light; microscope.

1. INTRODUCTION

Thermal spray techniques, such as plasma- or combustion-heated, have a history of more than a century [1]. In recent years, it has become an increasingly important technology to protect metal surfaces, in most cases ferrous materials, from erosion and/or wear of important infrastructures which require longevity [2-4] such as electricity transmission towers and bridges. The thermal spray process is carried out in three steps. The first step is to pre-treat an originally smooth metal substrate surface by roughening it to more than a few tens of μm. The second step is to check whether the pre-treated surface satisfies the necessary requirement, while in the final step a coating layer is formed by spraying thermally molten droplets over the pre-heated surface. The coating qualities, such as adhesive strength and porosity, are known to be much influenced by pre-treated surface conditions as well as by the velocities and temperatures of the impinging molten droplets [5].

These three spray steps take almost about the same lengths of time (which depend on the coated areas and the environments of the spray procedures being carried out), because the second step is usually carried out using a surface roughness tester [6], which requires a long measuring time by experienced technicians. If an optical method is developed to yield reliable data in a fast way, the time necessary for the full thermal spray process may be shortened to almost 2/3 of that of the time presently spent, namely by almost eliminating the second step. Bearing this in mind, many optical methods for the second step have been proposed [7], but none has emerged to the state of confidence to replace the surface roughness tester. This is mainly because so far those optical methods lack the ability of yielding sufficiently quantitative data.

The basic requirements of such an optical monitor may be summarized as (i) reasonably cheap, (ii) easy operation for laypersons, (iii) easy access to the targets to be investigated, and (iv) an *in-situ* capability, along with (v) the capability of yielding above-mentioned sufficiently quantitative information, which is equivalent in precision to those measured using the surface roughness tester.

The purpose of this article is to present a new method to improve on the drawbacks in the first report based on the same principle by the present authors [8,9], by using a more advanced instrument. This article is structured as follows: The employed method and equipment are described in section 2, the results that have been obtained are shown in section 3, the discussions based on the results, along with the necessary steps to bring the present instrument into an eventual surface monitor, are presented in section 4 and section 5 is a brief summary.

2. METHODS AND EQUIPMENT

2.1 Background

Substrate pre-treatments before spray processes are usually carried out by blasting surfaces of raw materials (usually iron and steel), so as first to remove dust and oxide layers, and then to form surface morphologies suitable for subsequent spray depositions. Removal of dust and oxide layers may be checked by eye-observation of experienced technicians, which does not take much time. However, the surface morphologies have to be checked quantitatively in terms of the surface roughness parameter R_z as defined by the addition of 'the height of the highest peak R_p and the depth of the deepest valley R_v' and R_a as defined by 'the root-mean-square average of a roughness' for roughness curves as shown in Fig. 1, over a length of 8 mm for the case of R_z having around or more than a few tens of μm [10]. The importance of those surface roughness parameters R_z and R_a on the resultant spray coating qualities, such as adhesion strength, was clearly identified in the recent references [11].

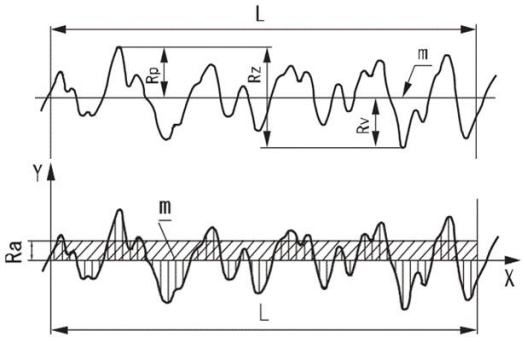

Fig. 1. Definitions of the surface roughness parameters R_z and R_a[10]

The most classical and simplest method of obtaining values of R_z and R_a is to use a surface roughness tester [6], in which a needle having a

small tip of about 2μm is traversed over the surface to register up and down motion of the needle. It is necessary to carry out the measurement with utmost attention, which requires laborious work by experienced technicians. To date, this is the only reliable quantitative method routinely employed in spray factories and fields.

Optical methods may substantially reduce the measurement times. In this respect, the 3D microscope [12] has been developed and commercialized, as shown in Fig. 2. In this instrument, well-collimated light is scanned over a surface at certain angles and reflected lights are observed using a microscope to yield the surface morphology by the triangulation method. It can give a detailed surface morphology of an area in a short time (around a few seconds). However, it has to be set on a stable table/desk and is very expensive, and thus is not suitable for use *in-situ* at spray factories and out in the field. Simpler methods have been proposed and tested [7], but none has emerged to the level of replacing the surface roughness tester. These are the reasons for proposing a new method in this article that is on the one hand fast and accurate enough, and on the other hand inexpensive.

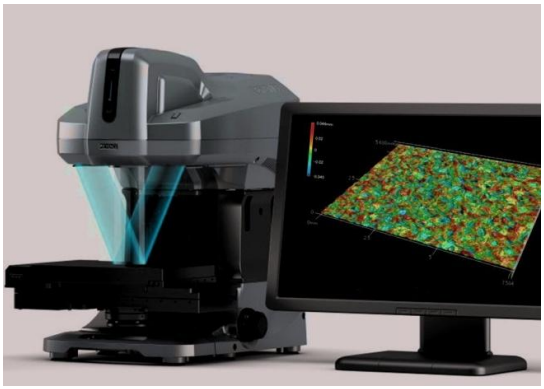

Fig. 2. 3D microscope (Keyence VR-3000) (left) and an example of a surface morphology obtained using it (right) [12]

2.2 Principle of the Proposed Method

Fig. 3(a) illustrates the schematic arrangement and the principle of the proposed method. A light beam from the upper right corner is shaped to have a width as narrow as possible, and a length of a few mm. This light beam illuminates the target surface (which has a height difference of *d* from the flat area as shown in (b). A microscope camera located at the top observes the diffusely reflected light from the target. Due to the surface morphology, the straight laser light is seen to be distorted as shown in the Figs. 3 (a) and (b).

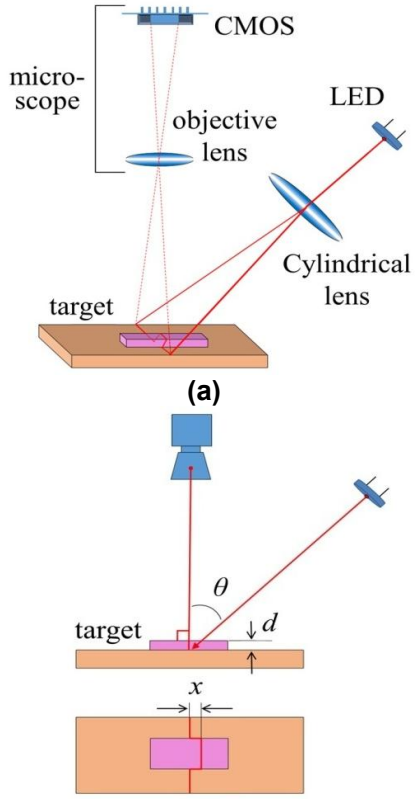

Fig. 3. Schematic arrangement (a) to show the principle of the proposed method, shown along with its geometry (b)

In order to obtain the value *d*, one may use the trigonometric relation for the symbols shown in Fig. 3(b) as follows:

$$d = x/\tan\theta \quad (1)$$

In fact, this principle is used in the 3D microscope described in section 2.1. This microscope was developed to obtain the three-dimensional information of an arbitrarily shaped object, utilizing Computer Tomography for the analysis. Namely, as can be seen in Fig. 2, two narrow-shaped light sources are used from two different directions, and the three-dimensional image of the object is reproduced using computer-aided tomography. In order for this instrument to function correctly, the alignment of two light beams illuminating the object has to be very accurately controlled, which can only be attained with a microscope placed on a solid and stable table.

On the other hand, the pre-treated surfaces for thermal spray have continuous minute up-down changes of a few tens to just above 100 μm over the flat surfaces of the substrates. In order to interpret the data from the actually measured pre-treated surfaces, the 'm' line in Fig. 1 has to be decided. This line is defined as yielding the same areas above and below it, as may be seen in the lower figure of Fig. 1. Therefore, one first draws a tentative straight line, which approximately satisfies such a definition from the recorded profile. Then, the areas above and below the tentative line are calculated. After iterative procedures to try to come to the same areas in the end, one comes to the correct 'm' line. The values of R_z and R_a are obtained by their definitions described for Fig. 1.

We assume the relationship of Eq. (1), which is rigorously valid for a step-like structure on a flat surface as shown in Fig. 3(b), to be applicable for the present case, using a single light beam as the first approximation. However, the applicability of this assumption has to be experimentally confirmed, along with its limitation. It is the purpose of this article, by carrying out an experiment using the present optical instrument against a surface roughness comparator [13], whose roughness is clearly specified. Also, blasted samples were measured using both methods based on the present optical instrument and a surface roughness tester [9], in order to see the degrees of the mutual agreement/disagreement.

2.3 Experimental Arrangement

The photograph in Fig. 4(a) shows the arrangement of the experimental apparatus. Here, the target mounted on a vertical holder at the upper-right end was illuminated at an irradiation angle of 45º by LED light from a source located at the bottom-left corner, as illustrated in Figs. 3(a) and (b). The LED (Hamamatsu L6108 [14], λ=670 nm) had a very small emission region of 0.25×0.25 mm^2. The radially-emitted LED light was formed into a parallel beam by separately collimating it in the horizontal direction and the vertical direction using two cylindrical lenses with different focal lengths of 30 mm and 150 mm, respectively. In order to eliminate weak scattered light surrounding the main part of the beam, two optical slits were also installed. A cylindrical lens with a short focal length of 15 mm was placed just in front of the target surface. The resulting width and the length of the irradiated LED light beam on the target surface were approximately 40 μm and 10 mm, in the horizontal direction and the vertical direction, respectively. The image showing the distortion due to the roughness of the target surface was captured by a microscope (Thanko, Dino-Lite Premier 2 S [15]) from directly above, and was analyzed using a personal computer. The photograph shown in Fig. 4(b) is the surface profile comparator, which is used to confirm whether the proposed method could differentiate the designated values for the segments of S1, S2, S3, and S4 (clockwise from upper left), where only the values of R_z were given as 24, 48, 87, and 137 in the unit of μm, respectively. On the other hand, the surface profile comparator was simply replaced by a blasted surface for the measurements of the latter.

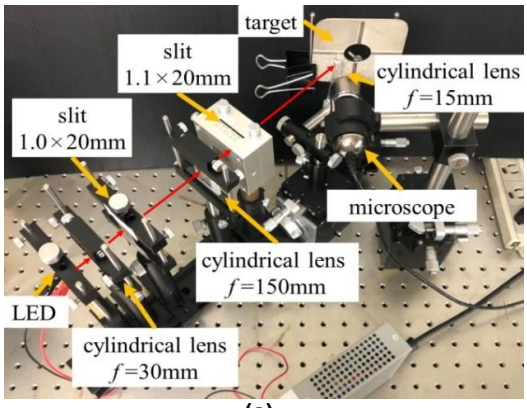

(a)

(b)

Fig. 4. Photographs of the experimental arrangement (a) where the red lines were added to the photograph to illustrate the LED light path, and of (b) the enlarged target (the surface profile comparator) having a square shape of 88 mm on the side with its segments starting from S1 at the upper left clockwise through S2 and S3 to S4

In a previous article by the present authors [8], He-Ne laser light (wavelength of 632.8 nm) was used, but the laser speckles, caused by its high coherence, did not allow a measurement accuracy below about 10 μm. Therefore, the above-mentioned LED light, which emits incoherent light, was used instead. In order to use the same optical components as used for the case of He-Ne laser, red LED light with a wavelength of 670 nm was used.

3. EXPERIMENTAL RESULTS

3.1 General Remarks

Since we refer in later sections back to the present paragraph, we have numbered them in the following:

Firstly, it is to be noted that we tried to make the LED light at the target surface as narrow as possible. However, the single cylindrical lens shown in Fig. 3(a), combined with the very tight optical constraint from the lens to the target, resulted in yielding its resultant width to be around 40 μm. Because this value is about the size of the roughnessof S2 as shown later, a roughness smaller than this line width may naturally buried inside it, such that they are not discernible as such. On the other hand, if small areas of roughness are located with their hill and valley at both sides at or around the boundaries of the LED line, they may be judged as a large single roughness, thus overestimating the roughness values. This is because the line distortion, as depicted in Fig. 3(b), has to be judged from the movements of the center line of both upper and lower edges of the LED light at its target surface. Because of these reasons, the boundary (which is, in principle, 'a straight line', but a further consideration is necessary as shown in the second point below) of the up-down changes of the upper edge of the LED light at the target surface was used for the movement of x in Fig. 3(b). The lower edge line of the LED light at the target surface was confirmed to yield almost the same values of R_z and R_a, compared with those obtained from the upper edge line.

Second, the CMOS camera in Fig. 3(a) discriminates the red color (R) of the LED light using color filters placed in front of the CMOS element. However, there is always some leak into the green (G) and blue (B) elements when R impinges on them, resulting in registering a finite amount of output in the G and B elements, even when only the red color impinges onto the CMOS element. The intensities of the R, G and B are specified by 256 gradations. Under such a situation, therefore, there has to be a criterion to judge where the boundaries of R of the above-mentioned upper edge of the LED light. For the results shown below, R-GB=80 was used as the criterion. Its implication and the result of a different R-GB value are discussed in section 4.2.

Third and finally, it is to be noted that a single photograph of the above LED light on the CMOS camera occasionally recorded anomalously large deviations on some pixel elements compared with the rest of the elements. The origin(s) of this deviation is not fully understood, but is tentatively interpreted as due to specular reflections from some edge of the surface roughness, perhaps caused by shot-to-shot fluctuations of spatial intensity distributions of the LED light. In order to overcome this difficulty, ten photographs were recorded at each position, and the intensities of these photographs were added up using aphoto-editing software (Adobe Photoshop [16]). The implication of this procedure, along with the effect of the number of added photographs on the final result, is discussed in section 4.2.

3.2 The Results Using the Surface Roughness Comparator As the Target

Figs. 5(a) and (b) illustrate the results obtained using the surface roughness comparator as the target shown in Fig. 4(a), where the values of R_z and R_a, respectively, obtained using the surface roughness tester [17] in the abscissa (x) are presented against those using the present optical instrument in the ordinate (y). The measurements were carried out at five different locations on the surface roughness comparator for the surfaces S1, S2, S3 and S4 shown in Fig. 4(b). Here, the implication of the arrow in a value of the optical measurement in S4 is discussed in section 4.1.

It is to be noted that the lines on which the measurements were made for the surface roughness tester and the present optical instrument were independently chosen but were not the same. Therefore, it is not possible to plot the one-to-one correspondences obtained from the two measurements (this point is further discussed in section 4.3). Thus, the measured points for the segments S1 to S4 obtained using the surface roughness tester were plotted on the lines of the averages of the measured values

using the present optical instrument, and *vice versa*. The ellipses in Figs. 5(a) and (b) are drawn to guide the eyes to illustrate the observed regions for the surfaces S1, S2, S3 and S4 from left to right in Figs. 5(a) and (b). Those regions indicate observed regions of roughness at five different locations on the surfaces S1, S2, S3 and S4.

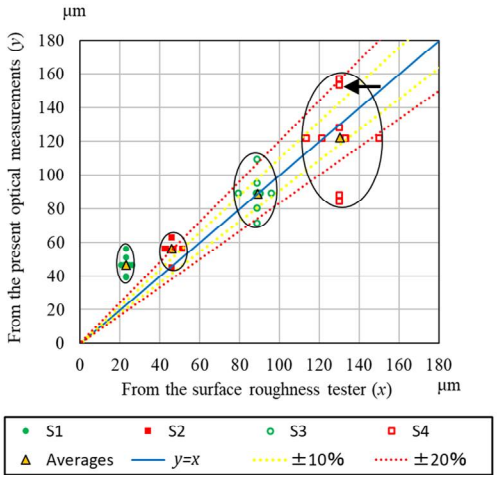

(a) R_z(Attenuation: 10%, R-GB: 80)

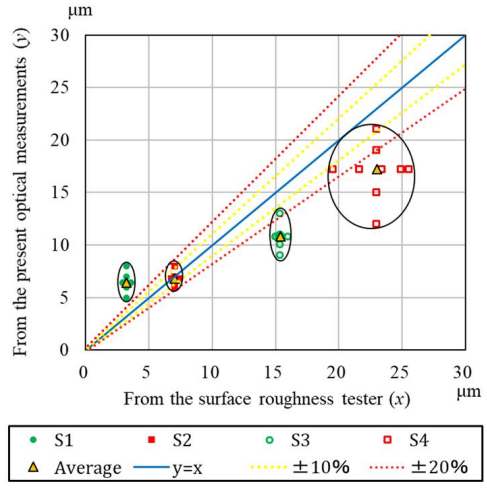

(b) R_a (Attenuation: 10%, R-GB: 80)

Fig. 5. Comparisons of the measured results of R_z (a) and R_a (b) obtained using the surface roughness tester (the abscissa) against those using the present optical instrument (the ordinate), using the surface roughness comparator as the target

In Figs. 5(a) and (b), the blue straight lines are drawn at 45°, implying the complete agreement (y=x) of measured results using both methods. The yellow and red dotted lines indicate departures from the complete agreement by ±10% and ±20%, respectively. One notices that the averages for the results using the surface roughness tester and the present optical measurements, shown by triangles in Figs. 5(a) and (b), are in good agreement for the segments S3 and S4. Also, the averages of both measurements agree well with those specified for the surface roughness comparator of 87 μm and 137 μm, for S3 and S4, respectively. However, some discrepancies are recognizable for S1 and S2, as the averages of both measurements are somewhat different from those specified for the surface roughness comparator of 24 μm and 48 μm, for S1 and S2, respectively. However, they are within allowable limits for such small roughness.

From the results shown in Figs. 5(a) and (b), one may conclude that the present optical method yields measured values of roughness nearly in accordance with those obtained using the surface roughness tester.

3.3 The Results Using a Blasted Surface as the Target

Figs. 6(a) and (b) illustrate the results obtained using blasted surfaces as the target (JISG-3101 SS400) in Fig. 4(a), prepared at the authors' factory as the test specimens, using the blasting cabinet (Atsuchi BA-1 [18]) with steel grid #70 sands. This figure has been constructed in the same way as Figs. 5(a) and (b). However, it is to be noted that the degrees of attenuation at the time of 10 measurements made at the same line of the LED light were increased from 10% for Figs. 5(a) and (b) to 25% in Figs. 6(a) and (b), because diffuse reflections from the blasted surfaces were found to be weaker than for the surface roughness comparator, described in section 3.2. This point is further discussed in section 4.3.

From the results shown in Figs. 6(a) and (b), one may once again conclude that the optical method yields measured values of the surface roughness roughly in accordance with those obtained using the surface roughness tester.

4. DISCUSSION AND CONCLUSION

4.1 About the Number of Accumulated Photographs

In the point 3 of section 3.1, a comment was made about the CMOS camera occasionally

recording a large deviation on some pixel elements compared with the rest of the elements. Therefore, ten photographs were recorded at each line of the observation. The intensities of these photographs were first attenuated by 1/10 and then added up using a photo-editing software to yield the results shown in Figs. 5 and 6.

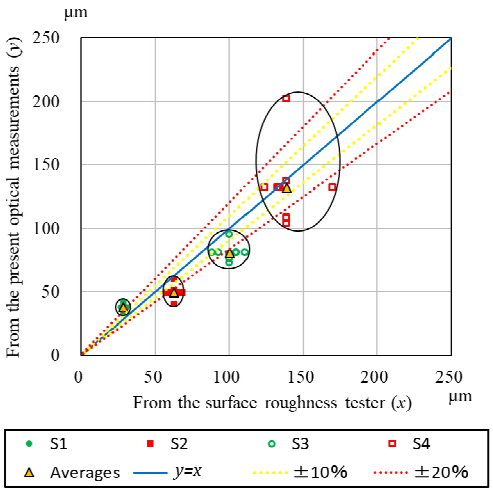

(a) R_z(Attenuation: 25%, R-GB: 80)

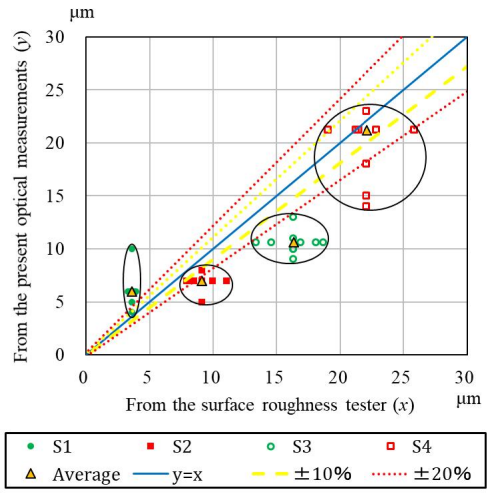

(b) R_a (Attenuation: 25%, R-GB: 80)

Fig. 6. Comparisons of the measured results of R_z(a) and R_a(b) obtained using the surface roughness tester (the abscissa) against those using the present optical instrument (the ordinate), for the blasted surfaces as the target

In order to see the effect of the number of recorded photographs, an exercise was carried out for the segment S4 of the surface roughness comparator, and the results are shown in Fig. 7. Here, the ranges of the observed values of R_z are shown in the ordinate against the numbers of added photographs in the abscissa. All ten photographs were used for the added number 1 (the far-left of the abscissa) yielding ten values of R_z. For the next added number 2, the intensities of these ten photographs had first been attenuated by 50%, from which randomly selected pairs were been attenuated by 50%, from which randomly selected pairs were then added using the photo-editing software to yield ten photographs, implying that all possible pairs from the ten photographs were not used, in order to see the same number of the R_z values for this case as for the added number 1. For the case of the added number 3, the intensities of the initial ten photographs had first been attenuated by 33%, from which randomly selected three were then added using the photo-editing software to similarly yield ten photographs. These procedures were continued until the added number 10, for which case all ten photographs were used, yielding a single point there. The last case corresponds to the arrow in Figs. 5(a) and (b). The error bars at all measurement points indicate the resolution limit of about ±4 μm, determined by the size of a pixel in the CMOS camera.

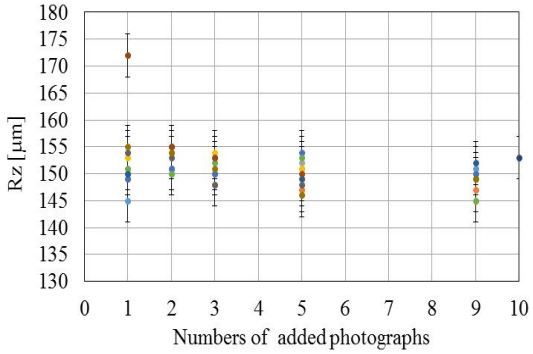

Fig. 7. Ranges of the observed values of R_z in the ordinate shown against the numbers of added photographs in the abscissa.

From the results in Fig. 7, we see that the large scatter of the measured results of R_z for the case of the added number 1 rapidly converges to the final value for the case of the added number 10. However, because there may be cases of more pixels than the above exercise case yielding large deviations from the rest of the CMOS elements, we conclude it to be more prudent to obtain a reliable measurement, to take ten

photographs and add them all up after attenuating by 1/10.A similar procedure was taken for the case of the determination of R_a.

4.2 About R-GB Values

As described in the point 2 in section 3.1, the magnitudes of the R, G and B signals of a single pixel of the CMOS elements are specified by 256 gradations, with each step having linearly increasing intensity with an increasing number. In order to look at 'how red' a particular pixel is, one has to specify a value of R-GB, which is defined as the minimum number of either R-G or R-B. For example, for R=203 with G=133 and below, it is specified as R-GB=70, if B is any number below 133. If R-GB increases, 'the degree of redness' increases. However, if one chooses too high a value of R-GB, there may be a possibility that there are too many points being missed out from the upper edge line of the LED light to be used to decide the value of x in Fig. 3(b), resulting in the determination of the upper edge line difficult. On the other hand, if one chooses too low a value of R-GB, the discrimination of R from G and B may also become difficult. Therefore, there is an optimum range of R-GB values for a particular photograph.

For the cases shown in Figs. 5 and 6, the value R-GB=80 was selected, where 10 photographs had first been attenuated by 50% and then added using a photo-editing software. If the above 10 photographs for the case of Figs. 6(a) and (b) were first attenuated by 25% and then added, the resulting photograph has two times higher intensity at each pixel. Then, the R-GB values higher than 80 for the case of Fig. 6 become more suitable. In Figs. 8(a) and (b), the R-GB value of 120 was chosen. If two figures 6 and 8 are compared, one sees that they give very similar results, except for minor details.

4.3 For Further Studies

With regard to the remark made in section 3.2, namely, to see the effect of measurements of the present optical instrument and the surface roughness tester being carried out on different lines of observation, a simulation study is now in progress. Here, the obtained values of R_z using the present optical measurements are to be compared with the computer-reconstructed surface roughness obtainable by traversing a cone-circular tip, having different shapes and angles. This study will be published in a separate article in future.

Finally, the following items have to be taken into consideration for the present optical method to be brought into an eventual surface roughness monitor to be used at spray factories and out in the field.

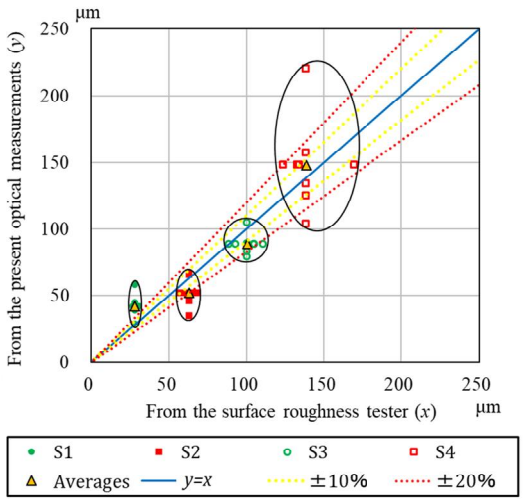

(a) R_z(Attenuation: 50%, R-GB: 120)

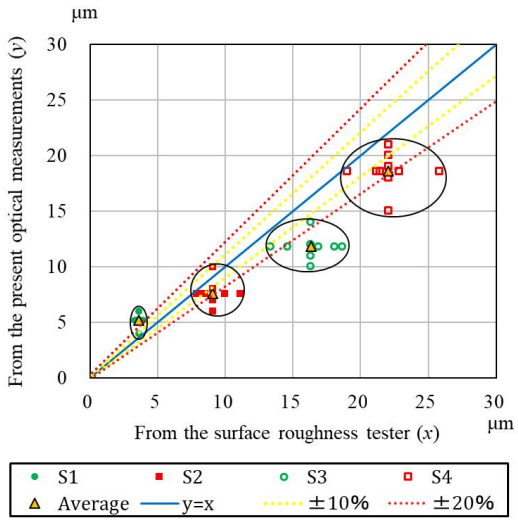

(b) Ra (Attenuation: 50%, R-GB: 120)

Fig. 8. The same photographs as figure 6 but treated differently as the intensities of 10 photographs were attenuated by 50% (against 25% for figure 6) then added and, the value of R–GB was increased to 120 (against 80 for Fig. 6)

4.3.1 The hardware

The present experiments were carried out on an optical bench as shown in Fig. 4(a). For the

actual surface roughness monitor, the optical system has to be set on the surface to be investigated. For this purpose, the optical system shown in Fig. 3(a) has to be fixed on a semi-spherical or semi–cylindrical surface, and its flat side is to be set on a surface to be investigated.

4.3.2 The software development

In the present experiments and analyses, manual work was necessary to obtain the results shown in Figs. 5, 6, 7, and 8. To avoid this and to speed-up the procedures *in-situ*, an automated analysis software has to be developed to analyze measured data of the surface roughness instantaneously *in-situ* at spray factories and out in the field.

4.3.3 The brightness test procedure

As evident from Figs. 6, 7, and 8, intensities of diffuse reflection from different surfaces are significantly different from others. Therefore, a test procedure has to be set up to check the proper attenuation of the observed numbers of photograph, which has to be incorporated with the selection of the R-GB value. Incidentally, while the present experiments were performed using a red LED light, other colors may be employed if necessity arises in different circumstances or environments.

5. SUMMARY

A simple optical method was shown to provide a new and versatile method to instantaneously yield a value of surface roughness of a blasted surface prepared for the subsequent thermal spray *in-situ*. Here, an LED light source was used along with a microscope camera to collect necessary data.

First, the proof-of-principle tests were performed against the surface roughness comparator, where the obtained roughness parameters R_z and R_a were compared with those using the surface roughness tester. Both results showed good accordance. Then, blasted surfaces were measured using both methods, again yielding general agreements.

Based on these results, the necessary steps were mentioned to further develop the present instrument into a reliable surface roughness monitor for use at spray factories and fields *in-situ*. These include further development of both hardware and software, along with a brightness test procedure caused by different diffuse reflection intensities from different materials and surface conditions.

It is the authors' hope that the present simple optical method will become a useful tool for thermal spray procedure as soon as possible, by shortening the working time to almost 2/3 of the presently necessary.

ACKNOWLEDGEMENTS

The authors want to express their gratitude for the instruction of Prof. Yuji Oki of Kyushu University with regard to the effect of laser speckles on the measurement accuracy in the case when a He-Ne laser was used as a light source in their former experiment. They would also deeply thank Prof. dr. Anthony Donné of the EURO fusion consortium, for his thorough reading of the original draft of this article and for his numerous useful/constructive comments and suggestions, which has resulted in rewriting it into the present more understandable contents with much clearer explanations.

COMPETING INTERESTS

Authors have declared that no competing interests exist.

REFERENCES

1. Vardelle A, Moreau C, Akedo J, Ashrafizadeh H, Berndt CC, Berghaus JO, et.al. The 2016 Thermal Spray Roadmap, J Therm. Spray Technol. 2016;25(8): 1376-1440.
2. Nataly C, Paul S. Thermally Sprayed Aluminum Coatings for the Protection of Subsea Risers and Pipelines Carrying Hot Fluids, *Coatings;* 2016; *6*(4):58.
3. Fauchais P, Vardelle A. Thermal Sprayed Coatings Used against Corrosion and Corrosive Wear. In: Jazi HS editor. Advanced Plasma Spray Application. INTECH Open Access Publisher, Rijeka, Croatia; 2012.
4. Fauchais P, Vardelle PM, Vardelle A. Reliability of plasma-sprayed coatings: monitoring the plasma spray process and improving the quality of coatings. J. Phys. D: Appl. Phys. 2013;46 (22):1-16.
5. Kawaguchi Y, Miyazaki F, Yamazaki M, Yamagata Y, Kobayashi N, Muraoka K. Correlations of coating qualities deposited using three different thermal spray technologies with measured temperatures

and velocities of spray droplets ejected from their guns, Coatings; 2017; DOI:10.3390/coatings7020027.

6. Yoshida I. Surface Roughness - Part 4, Mechanics, Design and Measurement Principles on Sensor of Contact Stylus Profiler, and Quality Use of Mechanisms -, J. Jpn. Soc. Precision Engrg. 2016; 82(2):142-147 (in Japanese).
7. Fukatsu H. Optical Profiling Techniques for Engineered Surface Topography, J. Jpn. Soc. Precision Engrg. (in Japanese). 2010; 76(9):995- 998
8. Kawaguchi Y, Kobayashi N, Yamagata Y, Miyazaki M, Yamasaki M, Muraoka K. Optical monitoring systems for thermal spray processes: droplet behavior and substrate pre-treatments. J. Instrum; 2017. DOI: 10.1088/1748-0221/12/11/C11031.
9. Jpn. PAT 2019-168353A: The measurement equipment and method of a surface roughness (in Japanese); 2019.
10. ISO 4287:1997. Geometrical Products Specifications (GPS) - Surface texture: Profile method – Terms, definitions and surface texture parameters.1997;4. (Accessed 15 May 2020) Available:https://www.iso.org/standard/10132.html.
11. Bobzin K, Öte M, Knoch MA. Surface Pre-treatment for Thermally Sprayed $ZnAl_{15}$ Coatings.J. Therm. Spray Technol. 2017; 26(3):464-472.
12. Keyence. Wide-Area 3D Measurement Head. 2016. (Accessed 15 May 2020) Available:http://www.keyence.com/products/measure-sys/3d-measure/vr-3000/models/vr-3200/
13. ISO 8503-1:2012 Preparation of steel substrates before application of paints and related products – Surface roughness characteristics of blast-cleaned steel substrates – Part 1: Specifications and definitions for ISO surface profile comparators for the assessment of abrasive blast-cleaned surfaces. 2012.12. Accessed 15 May 2020. Available:https://www.iso.org/standard/51979.html
14. Hamamatsu. Red LED L6108. (Accessed 15 May 2020) Available:https://www.hamamatsu.com/jp/en/product/type/L6108/index.html
15. Thanko. Dino-Lite Premier2 S. 2017. (Accessed 15 May 2020) Available:https://www.thanko.jp/shopdetail/000000000207/ct88/page1/recommend/
16. Adobe. Photoshop. Accessed 15 May 2020. Available:https://www.adobe.com/products/photoshop.html
17. Mitutoyo. Surftest SJ-210 Series. (Accessed 15 May 2020) Available:https://ecatalog.mitutoyo.com/Surftest-SJ-210-Series-178-Portable-Surface-Roughness-Tester-C1794. aspx
18. Atsuchi. ASCON blast machine BA-1 (in Japanese). (Accessed 15 May 2020) Available:http://www.atsuchi-ascon.co.jp/blast_cabinet/multipurpose_direct.html.

Peer-review history:
The peer review history for this paper can be accessed here:
http://www.sdiarticle4.com/review-history/57147